Exposure strategies for polymethyl methacrylate from *in situ* x-ray absorption near edge structure spectroscopy

X. Zhang,[a] C. Jacobsen, S. Lindaas, and S. Williams[b]
Department of Physics, State University of New York at Stony Brook, Stony Brook, New York 11794

(Received 29 November 1993; accepted 25 May 1995)

We have observed the chemical changes in PMMA irradiated by x rays *in situ*. The chemical changes are monitored by micro-x-ray absorption near edge structure spectra at the carbon absorption edge. The loss of the ester group (C═O) and formation of C═C bonds have been determined quantitatively from changes in the intensities of the respective π^* resonant peaks as a function of dose. Samples prepared under different conditions were examined. From the dose dependence of bond formation, scission and linking, the performance of the resist can be predicted, so that the preparation strategy, dose, and development can be optimized. © *1995 American Vacuum Society.*

I. INTRODUCTION

Poly(methyl methacrylate) or PMMA is probably the highest resolution organic photoresist used for UV, electron, and x-ray lithography, with ~10 nm lines having been fabricated using electron beam lithography on a thick substrate.[1] PMMA is also used as a high resolution recording medium for x-ray contact microradiography[2] and holography.[3] PMMA is a long chain molecule with a monomer structure shown in Fig. 1. Upon exposure to ionizing radiation (>4.3 eV typically), both the main chain and bonds to side groups can be scissioned.[4] This radiolysis lowers the local molecular weight and makes the exposed region more sensitive to dissolution in liquid developer. This behavior does not extend to infinite dose, however; at higher exposure, cross linking in PMMA starts to dominate and the resist becomes less soluble.[5,6] For lithography, one would like to completely remove PMMA from exposed areas, whereas for microscopy and holography one would like to have a quantifiable relationship between exposure level and developed thickness as well as the transition dose for cross linking dominance. It is commonly believed that postspin baking can affect this transition point, but we are unaware of previous data to quantify this trend.

Scission, cross linking, and other underlying chemical phenomena in exposed PMMA have been studied using many different methods. Dissolution rate curves[5,6] have shown that PMMA is a positive resist until very high dose levels are reached. The chemistry of exposed but undeveloped PMMA has been studied using Raman spectroscopy[7] and nuclear magnetic resonance (NMR);[8] these latter methods show the dependence of C═C and C═O bond densities on dose, and these parameters shed more light on the process than dissolution rate curves alone.

We describe here the use of carbon x-ray absorption near edge structure (XANES) spectra (280–310 eV) to examine the radiation effects on PMMA exposed to soft (317 eV) x rays. We have quantitatively monitored the chemical changes of PMMA prepared under different post-spin baking temperatures, and have attempted to predict the final performance of the resist using this information. Studies have shown that chain scission often results in the loss of C═O bond in the ester group with accompanying C═C bond formation.[8] The C═O bond loss will give rise to a reduction in the intensity of the corresponding π^* resonance. Cross links result in the formation of additional C═C bonds, giving rise to a π^* resonance at a different energy. Changes in the intensity of the π^* resonance as a function of dose can be monitored through carbon edge XANES (see Fig. 2) using the same apparatus which generates the radiation exposure. C-XANES provides the capability of observing the evolution of PMMA chemistry as a function of exposed dose *in situ*, supplying the information needed to optimize exposure strategy and PMMA preparation.

II. EXPERIMENTAL METHODS

A. The scanning transmission x-ray microscope

Our experiments make use of the scanning transmission x-ray microscope (STXM) at the X-1A beamline at the National Synchrotron Light Source, Brookhaven National Laboratory.[9] The microscope uses the high brightness soft x-ray beam produced by a soft x-ray undulator which is monochromatized with $\lambda/\Delta\lambda$ variable between 300 and 1000 (higher monochromaticity at the cost of lower flux can be selected by reducing the size of the monochromator slits).[10] The monochromatic x rays are focused to a 55 nm Rayleigh resolution spot using a Fresnel zone plate.[11] The instrument can either be operated in imaging mode as a scanning transmission x-ray microscope, or in micro-spectral mode where the photon energy and zone plate to specimen distance are scanned while the specimen remains fixed to acquire a transmission spectrum of a submicron area.[12] The sample sits in a helium gas environment to minimize air absorption, and the transmitted photon flux is measured using an efficient gas flow proportional counter. The microscope has considerable flexibility to accommodate different experiments. Figure 3 illustrates its ability to write a pattern into PMMA at high dose, and to subsequently image the pattern at low dose to read the mass loss out.

[a]Author to whom correspondence should be addressed.
[b]Present address: Boyer Center for Molecular Medicine, Howard Hughes Medical Institute, Yale University, New Haven, CT 06510.

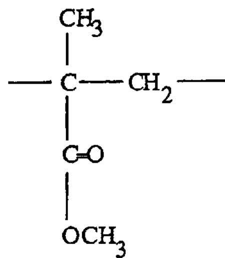

FIG. 1. Monomer structure of PMMA. The molecular weight of PMMA in this study is 9.7×10^5 Daltons, so each PMMA polymer chain contains 9700 monomers on average.

B. Atomic force microscope

X-ray transmission through a film depends both on atomic cross section and density of the film. We therefore wished to examine both the thickness and the mass thickness (x-ray transmission) of exposed PMMA. The former measurement was performed using an atomic force microscope to measure the surface profile of PMMA. This AFM is customized to have a highly linear (1 part in 5000) and long range $(75\ \mu m)^2$ scanning stage for use in reading out x-ray holograms.[13] The z axis is a normal piezoelectric scanner with 10 μm range; therefore, it is subject to hysterisis and measures height to an absolute accuracy of only about $\pm10\%$.

C. PMMA film preparation

In order to perform absorption spectroscopy, we needed to place PMMA films on a soft x-ray transmissive substrate. By backetching the silicon from silicon nitride coated wafers,[2] we are able to produce 100 nm thick, $(3\ mm)^2$ area silicon nitride windows which transmit ~60% of the incident beam. The PMMA films were spun at 4.5 krpm from a solution 4% by weight in chlorobenzene. This resulted in PMMA films approximately 0.3 μm thick. These were either used unbaked following several days of drying, or baked in air at temperatures of 150 or 200 °C for 2 h. The oven temperature was controlled to ±2 °C.

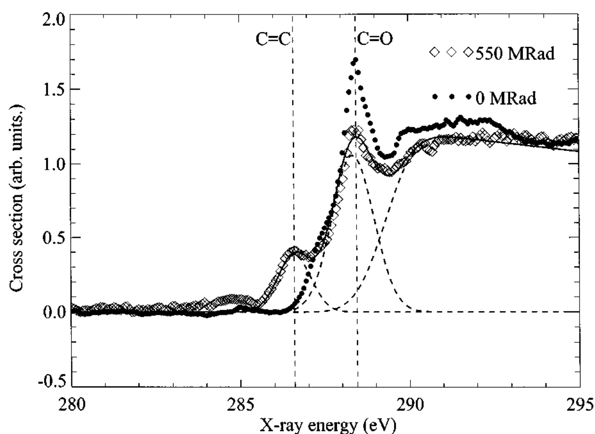

FIG. 2. Comparison of C-XANES of PMMA, baked at 150 °C for 2 h, before and after exposure; solid dots(●): before exposure, the peak from C═O bonds is strong while there is no obvious peak from C═C bond; diamond points(◇): after 550 Mrad exposure, the peak from C═O bond is weaker and the peak from C═C bond is stronger. The dashed lines show the fit using a rounded step function representing the absorption edge, and Gaussian functions for π^* resonance peaks. The solid line shows the total fit that agrees well with the raw spectra (diamond points). The energy calibration is accurate to 0.3 eV.

FIG. 3. (a) Letters etched into PMMA using STXM with 700 Mrad dose. The scanning stage was programmed to move the sample to write with the stationary x-ray focus. The transmission x-ray image (20 Mrad) shows substantial mass loss. (b) Atomic force microscope image of the area etched by x rays. The lines to the left of the letter "X" are due to beam exposure during the computer-data-transfer time between scan lines. The AFM image data has been left–right inverted to match the STXM image, and the rotation is due to remounting of the specimen from the STXM to the AFM stage.

D. Experimental methods

We used the imaging mode of the STXM to expose the resist, and the microspectral mode to measure carbon XANES in the exposed region. An image pixel size of 30 nm (half the 55 nm FWHM probe size) was used during expo-

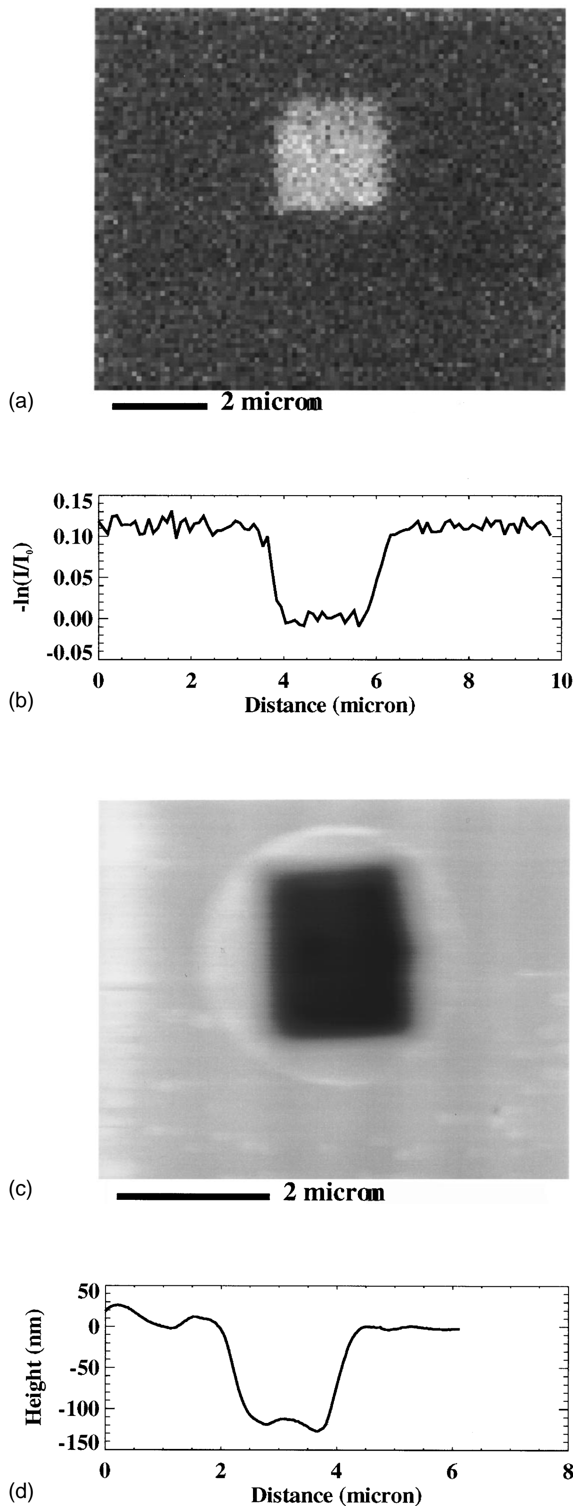

FIG. 4. (a) The STXM image of the dosed area surrounded by unexposed area. The light square in the center shows substantial mass loss. (b) Mass thickness profile [$\Delta(\mu\rho t)=-\ln(I/I_0)$]. (c) The same exposed area imaged by the atomic force microscope. (d) The thickness profile measured by the atomic force microscope.

sure to ensure even irradiation. Using 400 and 100 μm entrance and exit slits on the beamline monochromator, we were able to obtain a detected transmission count rate of 500 000 photons/s of 317 eV x rays with $\lambda/\Delta\lambda=450$ in imaging mode. By measuring the transmitted flux rate without the sample, the incident flux at the specimen plane can be calculated. The dose to the resist was controlled by adjusting the pixel dwell time in the microscope control software, and by adjusting the monochromator exit slit. We were typically able to expose a (10 μm)^2 area to 25 mJ/cm^2 in 5 min. In micro-spectral mode, we were able to take an absorption spectrum within that (10 μm)^2 exposed area over a range of 280–310 eV with 0.5 eV resolution in less than a minute. The beam was defocused to ~2 μm FWHM during spectrum acquisition to ensure that the maximum resist exposure of 0.1 mJ/cm^2 was kept acceptably small (<1%) compared to the exposure in imaging mode.

The dose to the PMMA layer can be calculated as

$$\text{dose}=\frac{I_0 TEA\, 1.6\times 10^{-8}}{dx\ dy\ t\rho}\ \text{Mrad}, \tag{1}$$

where I_0 is the measured incident flux in KHz, T the pixel dwell time in ms, $A=1-e^{-\mu t}$ is the fraction of x rays absorbed by the sample, E, the photon energy in eV (which is 317 eV for all exposures), $(dx\ dy)$ is the exposed area in μm^2, t is the thickness in μm, and ρ the density of the sample in g/cm^3. The $1/e$ absorption length is

$$\mu^{-1}=2r_e\lambda\ \frac{N_A}{A}\ \rho f_2, \tag{2}$$

where $r_e=2.812\times 10^{-15}$ m, N_A is Avogadro's number, A is the atomic weight, and f_2 can be found from tabulated values valid at wavelengths away from the immediate vicinity of absorption edges.[14]

During resist exposure, we delivered a dose ranging from 50 to 150 Mrad per image by varying the dwell time, and 15–25 such images in the same area allowed us to deliver a final cumulative dose of 2000–2500 Mrad. Between each exposure, we acquired a carbon XANES spectrum from within the exposed area. Finally, we imaged the exposed area and some of the unexposed surrounding area at the completion of the experiment; since the exposed area has greater transmission as a result of mass loss, the presence of a light square in uniformly dark surroundings provided confirmation of the position reproducibility of the resist exposure [Fig. 4(a)]. Two pairs of measurements by x-ray transmission and by the atomic force microscopy are compared to determine the density dependence with dose. The mass thickness losses [$\Delta(\rho t)$] measured by x-ray transmission give values of $(0.112\pm 0.002)/\mu_m$ and $(0.122\pm 0.003)/\mu_m$ [the latter one was shown in Fig. 4(b)] separately for two differently dosed areas, where μ_m is the mass absorption coefficient at this wavelength. Figure 4(c) is the same area as in Fig. 4(a) imaged by the atomic force microscope, where the thickness differences between exposed and unexposed area for those two differently dosed areas are 119.5±0.2 and 134.3±0.2 nm separately [Fig. 4(d) is the line profile corresponding to Fig. 4(b)]. The ratio between the mass thickness measurement to thickness is

$$\frac{\frac{\Delta(\rho_1 t_1)}{\Delta(\rho_2 t_2)}}{\frac{\Delta(t_1)}{\Delta(t_2)}}=\frac{\frac{\Delta(\rho_1)t_1+\rho_1\Delta(t_1)}{\Delta(\rho_2)t_2+\rho_2\Delta(t_2)}}{\frac{\Delta(t_1)}{\Delta(t_2)}}=1.03\pm 0.05.$$

This result is consistent with the assumption that the mass loss is mainly due to thickness loss, and the density of the resist does not change appreciably with dose so that $\Delta(\rho_1)=\Delta(\rho_2)=0$, *and* $\rho_1=\rho_2$.

E. Data analysis

Absorption spectra are determined by the thickness of the sample, t, and the linear absorption coefficient, μ (which is the inverse of the $1/e$ attenuation length), as

$$I(E)=I_0(E)e^{-\mu(E)t}, \tag{3}$$

where I is the transmitted flux at energy E and I_0 is the corresponding incident flux. The optical density can then be determined from

$$-\ln(I/I_0)=\mu t, \tag{4}$$

where I and I_0 are experimental data. Spectra are then fitted using a nonlinear least-square fit to a combination of a rounded step function representing the elemental absorption edge, and Gaussian peaks for the π^* resonances as shown in Fig. 2. The step function is the integration of a Gaussian function,[15]

$$I_{\exp}=H\left[\frac{1}{2}+\frac{1}{2}\,\mathrm{erf}\left(\frac{E-P}{\Gamma_G/(2\sqrt{\ln 2})}\right)\right], \tag{5}$$

where P is the position of the inflection of the step (in eV), H is the height of the function immediately above the step, and Γ_G is the FWHM of the step.

III. RESULTS

Figure 2 shows the carbon XANES spectra from PMMA. The π^* resonance at the higher energy side which is present in both unexposed and exposed PMMA is from C═O bonds from the ester group in PMMA (the spectrum and peak assignment for unexposed PMMA can be found in Ref. 15). The π^* peak at lower energy is assigned to C═C bonds, mainly because studies by other methods[8] have shown that C═C bonds are formed in PMMA upon irradiation, while no other carbon double bonds which can give rise to a sharp π^* resonance have been reported; furthermore, the energy difference between these two peaks (2 eV) falls within the typical difference between π^* resonances of C═O and C═C bonds (1.5–2.5 eV).[15] The x-ray absorption coefficient at the π^* resonance is proportional to the density of the corresponding bonds. The peak intensities of the π^* resonance from C═O and C═C bonds as a function of dose are plotted in Fig. 5 for unbaked PMMA (UnP), PMMA baked at 150 °C for 2 h (150P), and PMMA baked at 200 °C for 2 h (200P). As expected, for all samples, the peak intensity from the C═O bond decreases and the intensity from C═C bond increases with dose.

The resist development rate depends on the net average molecular weight arising from chain scission and cross link-

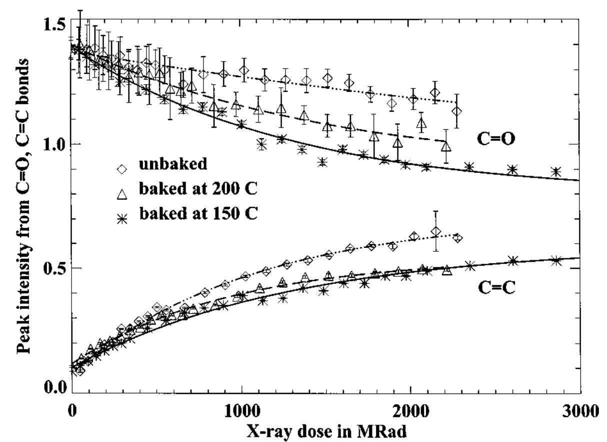

FIG. 5. C═C and C═O peak intensity changes for PMMA baked at 150 °C, PMMA baked at 200 °C, and unbaked PMMA. The curves are simple exponential fits [Eqs. (7)]. For PMMA baked at 200 °C, the peak from C═O decreases faster than that from unbaked PMMA and slower than that of the resist baked at 150 °C. For unbaked PMMA, the peak from C═C increases faster than that from baked PMMA. There are two sources of error in the data: photon statistics and curve fitting. There are over 1000 photons at most data points and over 400 photons at the sharp absorption peak, giving errors less than 5%. The fitting error is typically a few percent. The combined error is less than 10%.

ing as will be discussed later. From Fig. 5, we observe that the intensity of the C═O bond peak for sample 200P decays faster than that of sample UnP, but slower than that of sample 150P, suggesting that sample 150P has the most chain scission per dose among the three samples. The intensity of the C═C peak for sample 150P increases more slowly than that of sample UnP but at a comparable rate to that of sample 200P. This indicates that baked PMMA will have less cross-linking than unbaked PMMA for a given dose. PMMA baked at 150 °C develops main chain breaks more rapidly and cross linking less rapidly, so that it has higher sensitivity than unbaked PMMA. PMMA baked at higher temperature (200 °C instead of 150 °C) shows similar cross-linking development rate but less chain scission. Therefore, Fig. 5 suggests that PMMA baked at modest temperature will give the best sensitivity.

The mass thickness loss as a function of dose was measured directly from x-ray transmission at a photon energy of 317 eV (far from carbon-edge resonance, the attenuation length μ^{-1} is known).[14] The mass thickness changes exponentially with dose as is shown in Fig. 6, with unbaked PMMA showing the highest direct mass thickness loss per dose. The mass thickness loss as a function of dose is fitted to the equation

$$t_m=t_0[1-\exp(-D/D_m)]. \tag{6}$$

The fitted parameters t_0 (initial thickness) and D_m (characteristic dose) are summarized in Table I.

IV. DISCUSSION

Using the method described above, we have measured the spectral changes taking place in PMMA as a function of exposure to 317 eV soft x rays. We now wish to extract scaling relationships from these measurement, and consider

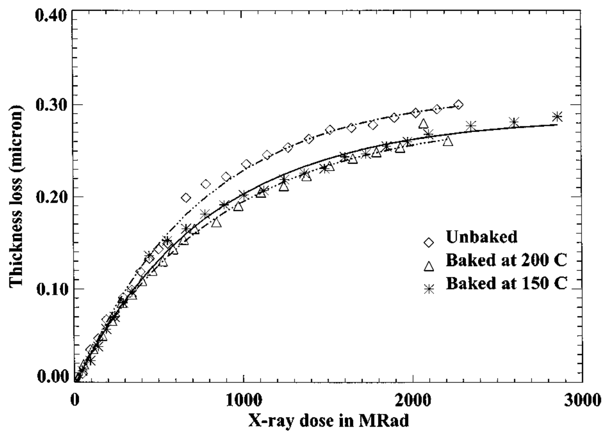

FIG. 6. Direct mass thickness loss vs dose. The curves are simple exponential fits from Eq. (6). The unbaked PMMA has a larger direct mass thickness loss than PMMA that is baked.

the implications for resist exposure and development. In the discussion below, we will use a simple first order approximation to model our data to obtain the molecular weight and dissolution rate which are the parameters characterizing PMMA performance and that can then be compared with direct measurement. This comparison can then be used to give us the relative efficiencies of chain scission and cross links (see discussion below) which provide a constraint on models for PMMA chemistry.

We model the peak intensities P associated with the C=O and C=C π^* resonance (obtained from measurements like those shown in Fig. 2) as a first order process,

$$P_{C=O}=A_s+B_s \exp(-D/D_s),$$
$$P_{C=C}=A_c+B_c \exp(-D/D_c), \quad (7)$$

where $P_{C=O}$ is the peak intensity of C=O bonds, and $P_{C=C}$ is the peak intensity from C=C bonds. The parameters A_s, B_s, D_s describe the C=O peak at 288.4 eV whose intensity reduction is associated with the chain scission. The parameters A_c, B_c, and D_c describe the C=C peak at 286.7 eV whose intensity increase is related to crosslinking. The data along with the fits of Eqs. (7) using the parameters in Table II are shown in Fig. 5. The peak intensities at zero dose are given by A_s+B_s, and A_c+B_c, respectively. Unbaked PMMA has the largest characteristic scission dose D_s, implying the lowest scission rate, while PMMA baked at 150 °C has the smallest characteristic dose, thus highest scission rate. PMMA baked at 150 °C shows the largest characteristic dose for crosslinking, D_c, indicating the slowest cross-linking rate. Our results of $D_s \approx D_c$ (see Table II) indicate that the rate of C=C bond formation is comparable to the rate of C=O bond loss for PMMA baked at 150 °C.

TABLE I. Fitted parameters for mass thickness loss according to Eqs. (6).

Sample	t_0	D_m (Mrad)
Unbaked	0.314±0.001	755± 9
Baked at 150 °C	0.287±0.002	807±12
Baked at 200 °C	0.285±0.002	881± 9

These results are in agreement with the results from Fourier transform infrared (FTIR) spectroscopy which indicate that for every ester group lost, there are 1.03 C=C bonds formed.[8] $A_s/(A_s+B_s)$ is the remaining fraction of C=O intensity after a large dose. Similarly, A_c is the peak intensity of C=C bonds after a large dose. Unbaked PMMA shows the largest A_c, so it will have the most cross links after a significant dose (saturation value for cross links) though PMMA baked at 200 °C shows the smallest characteristic dose D_c, thus the highest rate to reach the saturation value.

The peak intensities P were normalized to the height H of the non-XANES absorption step [Eqs. (5)] so that they are independent of resist thickness. The peak intensities P per normalized thickness (with dimension of length^{-1}) are therefore proportional to the number of corresponding bonds per unit volume, N. The constant of proportionality, σ, is the cross section from Fermi's Golden rule, which is the same for the π^* resonance from C=C and from C=O:[15]

$$N_{C=O}=\frac{1}{\sigma} P_{C=O},$$
$$N_{C=C}=\frac{1}{\sigma} P_{C=C}. \quad (8)$$

The number of PMMA macromolecules per unit volume is given by

$$N_{\text{polymer}}=\rho N_A/\text{MW}_0=7.32\times10^{17}\ \text{cm}^{-3},$$

where ρ is the initial density (1.18 g/cm^3), MW_0 is the molecular weight (9.7×10^5 Daltons in this study), and N_A is Avogadro's number.

The number of monomers per unit volume is

$$N_{\text{monomer}}=N_{\text{polymer}}\text{MW}_0/\text{mw}=7.10\times10^{21}\ \text{cm}^{-3},$$

where mw is the molecular weight of the monomer (100.12 Daltons). Each monomer contains one C=O bond, so we can find constant σ in equation 8 from $P_{C=O}$ at zero dose using (Eqs. (7))

$$\sigma=\frac{P_{C=O}(D=0)}{N_{\text{monomer}}}=\frac{A_s+B_s}{N_{\text{monomer}}}=1.95\times10^{-22}\ \text{cm}^3.$$

As noted before, chain scission will result in the reduction of C=O bonds and possible formation of the C=C bonds,

TABLE II. Parameters obtained for fitting the data of Fig. 5 to Eqs. (7).

Sample	A_s	B_s	D_s (Mrad)	A_c	B_c	D_c (Mrad)
Unbaked	0.80 ±0.03	0.58 ±0.03	5000±300	0.714±0.004	−0.633±0.004	1080±10
Baked at 150 °C	0.794±0.004	0.600±0.003	1310± 20	0.592±0.001	−0.489±0.001	1230±10
Baked at 200 °C	0.90 ±0.03	0.50 ±0.03	1520±140	0.545±0.002	−0.427±0.001	940±20

and cross links will result in the formation of C=C bonds. The possible chemical reaction channels PMMA can undergo upon irradiation have been reviewed in Ref. 8. Some of the non cross-linking channels will produce C=C bonds, while not all C=O bonds lost will cause chain scission. For simplicity, we assume that the nature of the chemical reaction mechanism for nonscissioned PMMA molecules is independent of dose over the dose range of interest, so the number of chain scissions events, N_s, will be proportional to the reduction of C=O bond per unit volume ($N_{\text{monomer}}-N_{\text{C=O}}$). Similarly, we assume that the broken PMMA molecules will combine with the same chemical channels over the dose range, so those nonscission-produced C=C bonds will have a constant portion of contribution from cross linking. The number of cross links, N_c, will then be proportional to the total number of C=C bonds formed minus those formed by chain scission. This gives

$$\begin{aligned} N_s &= C_s(N_{\text{monomer}}-N_{\text{C=O}}) = C_s(N_{\text{monomer}}-1/\sigma P_{\text{C=O}}), \\ N_c &= C_c(N_{\text{C=C}}-C_s' N_s) = C_c(1/\sigma P_{\text{C=C}}-C_s' N_s), \end{aligned} \tag{9}$$

where C_s is the fraction of C=O bond loss which cause chain scission, C_s' is the fraction of chain scission which produce C=C bonds, and C_c is the fraction of C=C bonds which are products of cross links rather than chain scission. Raman spectroscopy measurements[8] give $C_s=0.293$.

We will now consider only those chain scissions which break long chains (increasing molecular numbers per unit volume and thus decreasing the average molecular weight), and those cross links which link molecules together (decreasing the number of molecules per unit volume and thus increasing the molecular weight). Since we assume that the resist density ρ does not change with dose, we can write the dose dependent molecular weight MW(D) as

$$\text{MW}(D) = \frac{\rho N_A}{N_{\text{polymer}}+N_s-N_c}. \tag{10}$$

The dissolution rate, $R(D)$, generally increases with decreased molecular weight according to a power law dependence;

$$\begin{aligned} R(D) &= R_0\left(\frac{\text{MW}_0}{\text{MW}(D)}\right)^{\gamma} \\ &= R_0\Bigg\{1+\left(\frac{C_s}{N_{\text{polymer}}}\right)\Bigg[(1+C_cC_s') \\ &\quad\times\left(N_{\text{monomer}}-\frac{A_s}{\sigma}-\frac{B_s}{\sigma}\exp(-D/D_s)\right) \\ &\quad-\frac{C_c}{C_s}\left(\frac{A_c}{\sigma}+\frac{B_c}{\sigma}\exp(-D/D_c)\right)\Bigg]\Bigg\}^{\gamma}. \end{aligned} \tag{11}$$

Using Eq. (11), the experimentally determined values for A_s, B_s, D_s, A_c, B_c, D_c (Table II), $C_s=0.293$ as determined from Raman spectroscopy,[8] and using the calculated constants N_{polymer}, N_{monomer}, σ, we obtain the dissolution rate curves as plotted in Fig. 7. The curves are plotted for several different ratios of C_c/C_s, representing different relative efficiencies for cross links and chain scission for PMMA baked at 150 °C. When this ratio falls within the range $1>C_c/C_s>0.9$, the dissolution rate of exposed PMMA changes from increasing to decreasing at high dose, reproducing the behavior observed in other studies.[7] This model can be compared with direct thickness measurements of developed PMMA. Kubiak *et al.*[16] have used a stylus profilometer to measure the remaining thickness of PMMA which was baked at 160 °C for 1 h before exposure (we are unaware of published data for 2 h baking at 150 °C). Figure 7 and Fig. 8 show dissolved thickness data obtained by subtracting the thickness reduction due to mass loss (as determined in the present study) from the data of Kubiak *et al.* Figures 7 and 8 show that the dissolution rate model of Eq. (11) is in very good agreement with the data when $C_c/C_s=0.965$,

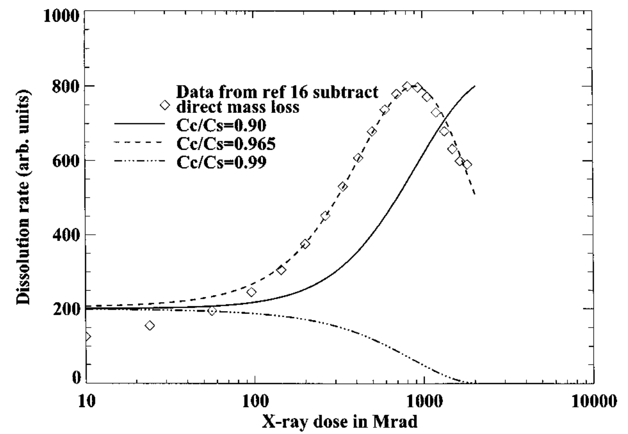

FIG. 7. Dissolution rate change with dose assuming different relative scission and linking efficiencies for PMMA baked at 150 °C for 2 h. The power law relationship between dissolution rate and molecular weight has been used. The MW in Eqs. (10) and the fitted parameters in Table II have been used. From our calculations and the profilometer data from Ref. 16, the best C_c/C_s is estimated to be 0.965 for PMMA baked at 150 °C for 2 h.

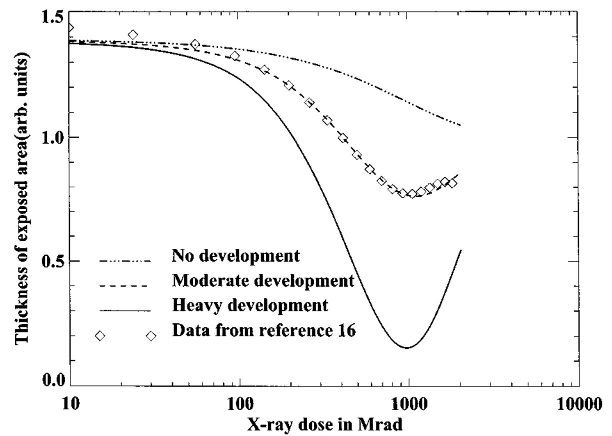

FIG. 8. Thickness of exposed area calculated after development for PMMA baked at 150 °C. The curves are obtained using Eqs. (11) and (10) with $\gamma=1.9$ and $C_c/C_s=0.965$. No development will give larger linear range and reduced contrast between exposed and unexposed areas. Moderate development (we have set $T\,R_0=140$ Å to make direct mass loss and dissolution contribute comparably to thickness change) and heavy development ($T\,R_0$ has been set to 340 Å to make thickness change from dissolution dominate) will result in better contrast at low dose, with reduced linear range. At high doses, the exposed part is less soluble, thus the contrast between the unexposed and exposed areas is reduced. Figure 8 also shows the result from Ref. 16.

$\gamma=1.9$, and $C_s' = 0.008$. The data and the model both indicate that the dissolution rate reverses at around 900 Mrad, and that this reversion dose is very sensitive to the ratio C_c/C_s as well as C_s' (when $C_s' > 0.05$, the reversion dose exceeds 1100 Mrad).

For lithography or microscopy applications, one is ultimately concerned with the remaining thickness, t_r, of PMMA as a function of absorbed dose D. This will be due to the combination of dissolution and direct mass thickness loss as was noted earlier. The remaining thickness is given by

$$t_r(D,T)=t_0-t_m(D)-TR(D), \tag{12}$$

where T is the liquid development time in seconds.

The remaining thickness as a function of dose is plotted in Fig. 8. The curves were obtained using Eqs. (12) and (11) with $\gamma=1.9$, $C_c/C_s=0.965$, and $C_s' = 0.008$. For moderate development, where we used $TR_0=140$ Å in our calculation, the thickness change comes from both direct mass loss and dissolution. If developed heavily ($TR_0=340$ Å in our calculation), dissolution is the dominant effect on final thickness, and will give better contrast at low doses. At very high dose, crosslinking dominates so that the exposed area is less soluble, reducing or even reversing the contrast.

V. CONCLUSION

We have demonstrated that direct chemical changes in PMMA due to x-ray irradiation can be monitored *in situ*. Since chain scission results in the loss of an ester group while cross linking yields the formation of additional C═C bonds, we are able to independently determine the relative rates of chain scission and cross linking for samples prepared under different baking temperatures and to predict performance qualitatively based on carbon XANES data. Once the relationship between bond formation and scission or cross linking is determined, one will be able to quantitatively predict the performance of the resist at different doses and for differently prepared samples, enabling the determination of the optimum exposure range and preparation condition.

Although we chose PMMA as a convenient and interesting example, this method can be applied to study radiation induced chemical changes in other resists or polymers in general. Furthermore, since our soft x-ray microscope has 50 nm spatial resolution at present, it can also be used to study the spatial structure of different resists as well as the dose and photon energy dependence of the structure. The relationship between XANES peak intensity and dose, can also be used for absolute dose measurement for x-ray lasers or laser plasma sources where the short, intense flash exposure makes other forms of measurement more difficult.

ACKNOWLEDGMENTS

The authors would like to thank Dr. John Gilbert for introducing us to PMMA chemical changes. Dr. Janos Kirz made numerous useful suggestions. They also want to thank the whole X1A group, especially Sue Wirick, for their help and support. This project is supported by NSF Grant No. DIR 9005893. It was carried out in part at the NSLS which is supported by the Department of Energy.

[1]Ochiai *et al.*, Jpn. J. Appl. Phys. Part 1 **30**, 3266 (1991).
[2]P-C. Cheng, in *X-ray Microscopy*, edited by P. C. Cheng and G. J. Jan (Springer, Berlin, 1987).
[3]C. Jacobsen, M. Howells, J. Kirz, and S. Rothman, J. Opt. Soc. Am. A **7**, 1847 (1990).
[4]J. H. O'Donnell, *Radiation Effects on Polymers* [ACS Symp. Ser. **475**, 402 (1991)].
[5]E. Spiller and R. Feder, in *X-ray Optics*, edited by H. J. Queisser, Springer Series in Applied Physics, Vol. 22 (Springer, Berlin, 1977), p. 35.
[6]E. M. Lehockey, J. D. Wice, and I. Reid, Can. J. Phys. **65**, 975 (1987).
[7]E. M. Lehockey and I. Reid, J. Vac. Sci. Technol. A **6**, 2221 (1988).
[8]J. A. Moore and J. O. Choi, *Radiation Effects on Polymers* [ACS Symp. Ser. **475**, 156 (1991)].
[9]For present application of STXM, see *Soft X-ray Microscopy*, edited by C. Jacobsen and J. Trebes [Proc. SPIE **1741**, (1992)].
[10]H. Rarback *et al.*, J. X-Ray Sci. Technol. **2**, 274 (1990).
[11]C. Jacobsen, S. Williams, E. Anderson, M. T. Browne, C. J. Buckley, D. Kern, J. Kirz, M. Rivers, and X. Zhang, Opt. Commun. **86**, 351 (1991).
[12]H. Ade, X. Zhang, S. Cameron, C. Costello, J. Kirz, and S. Williams, Science **258**, 972 (1992).
[13]S. Lindaas, M. Howells, and C. Jacobsen, in Ref. 9.
[14]B. L. Henke, E. M. Gullikson, and J. C. Davis, At. Data Nucl. Data Tables 181 (1993).
[15]J. Stöhr, *NEXAFS Spectroscopy*, Springer Series in Surface Science, Vol. 25 (Springer, Heidelberg, 1992).
[16]G. D. Kubiak *et al.*, OSA Proc. Soft X-ray Projection Lithog. **12**, 124 (1991).